DECEMBER 1993

FOM-INSTITUUT
VOOR
PLASMAFYSICA
RIJNHUIZEN

ASSOCIATIE
EURATOM-FOM

LOW-N IDEAL AND RESISTIVE MHD STABILITY OF JET DISCHARGES

MHD ANALYSIS OF JET SINGLE-NULL DISCHARGES BY EXTENDING AND APPLYING CASTOR

G.T.A. HUYSMANS AND J.P. GOEDBLOED

RIJNHUIZEN REPORT 93-218

REPORT ON JET CONTRACT
NO. JT2/10327

PROJECT LEADER: J.P. GOEDBLOED

This work was performed as part of the research programme of the association agreement of Euratom and the 'Stichting voor Fundamenteel Onderzoek der Materie' (FOM) with financial support from the 'Nederlandse Organisatie voor Wetenschappelijk Onderzoek' (NWO) and Euratom.

POSTBUS 1207
3430 BE NIEUWEGEIN
NEDERLAND
EDISONBAAN 14
3439 MN NIEUWEGEIN
TEL. 03402 - 31224
TELEFAX 03402 -31204

CONTENTS

PREFACE

JET discharges display pronounced MHD activity which requires a numerical tool for accurately calculating the dissipative MHD spectrum for measured equilibria. The spectral code CASTOR (Complex Alfvn Spectrum for TORoidal plasmas), which was recently extended to incorporate a plasma-vacuum- wall system, provides such a tool. Many high performance discharges, in particular the preliminary tritium experiment (PTE), are done in single- null configurations.

Therefore, the methods and tools need to be extended form up-down symmetry to more general geometry. In the context of MHD spectroscopy this requires:

i) the generalisation of the equilibrium solver HELENA,

ii) the construction of the appropriate flux coordinates and the calculation of the corresponding metric coefficients,

iii) the extension of the normal mode analysis to this more general geometry.

The described generalisation of the resistive MHD normal mode analysis has been introduced in the codes HELENA and CASTOR, tested and applied. The applications focus on the high performance discharges, e.g. on the crash near the beta limit, on Edge Localized Modes (ELMs)and on the up- down asymmetric pumped divertor configurations.

This report describes the work that has been performed under contract JT2/10327

1. INTRODUCTION

The relevance/importance of both local and global MHD stability limits in JET is increasingly recognised. The global MHD stability limit, i.e. the Troyon limit, is reached and even exceeded in discharges with a low toroidal field which aimed for high-β [1,2]. Also the high performance discharges of the preliminary tritium campaign, can reach relatively high values of β/β_{Troyon} of about 80% [3]. The maximum β in these high performance discharges is limited by the overheating of the target plates.

With the expected improvements of the target plates in JET in the new JET divertor phase, the contamination of the plasma by an influx of impurities will be delayed, and higher values of beta are likely to be obtained. In the high performance discharges of the preliminary tritium campaign, β reaches values at maximum 80% of the Troyon limit. It is therefore likely that future high performance discharges with the new JET divertor will also reach values of β close to the Troyon limit. In this new divertor geometry, the shape of the plasma boundary has changed considerably. The new shape has a pronounced single X-point. Also, the ellipticity is increased and the triangularity of the plasma boundary has become much smaller. These changes in the plasma shape will have a large effect on the MHD stability limits.

In the first part of this report a study of the ideal MHD stability properties to ballooning modes and the $n = 1$ external kink mode of two of the new JET divertor geometries, the so-called 'slim' and 'fat' configurations, is presented. The stability calculations of the external kink mode of the single X-point plasmas required the extension of the equilibrium and stability codes HELENA and CASTOR to general non up-down symmetric plasma shapes. The new versions of HELENA and CASTOR are discussed in the appendices.

MHD stability is, however, not only important in plasmas close to the global ideal MHD stability limits which only indicate a maximum achievable β. In experiment, local stability criteria will become important well below the global stability limit. One example of a local stability criterion being exceeded is the occurrence of edge localized modes (ELMs). ELMs are driven by the local steepening of the profiles, i.e. the pressure and the current density profiles during the H-mode phase. They can be triggered by lowering the edge temperature by gas puffing and they can be stabilised by heating the plasma edge. ELMs can also be triggered by a strong impurity influx into the plasma. From this dependence of the occurrence of ELMs on the parameters influencing the edge resistivity it is concluded that the ELM is a resistive MHD perturbation.

One MHD instability that is likely to be important for the ELM precursor is the

free boundary resistive kink mode. In a study of the stability of the $n = 1$ free boundary tearing mode of a JET elmy H-mode equilibrium it was shown [2,4] that a small change in the current profile at the edge, increasing the edge current density gradient, can drive this mode unstable. Also, a critical value of the resistivity exists below which the mode is stabilised due to the favourable average curvature.

In the second part of this report we will extend this study in two directions. Firstly, higher values of the toroidal mode number ($n = 1..4$) are studied. Secondly the influence of the edge pressure gradient which will be more important for the higher mode numbers is discussed. For the stability calculations the CASTOR code [5] is used to solve the linear resistive compressible MHD equations for general axisymmetric equilibria. The equilibria and the mapping to the flux coordinate system used in CASTOR are calculated with the HELENA code [6].

2. IDEAL MHD STABILITY LIMITS OF THE NEW JET DIVERTOR GEOMETRY

In JET, β values close to and even exceeding the classical Troyon limit ($\beta_{max} = 2.8I[MA]/a[m]B_0[T]$), have been obtained in discharges with a low toroidal magnetic field ($B_0 \sim 1 - 1.5T$). At low toroidal field, the power needed to reach the β limit is relatively small so that overheating of the target plates and the subsequent impurity influx is not a limiting factor. In these high-β discharges the maximum β is limited by MHD events.

Recently, in the preliminary tritium campaign [3] β values have been obtained of maximum 80% of the Troyon limit at normal values of the toroidal field ($B_0 \sim 3T$). In these high performance discharges, the high-β values have been reached because of the large confinement time of the hot-ion H-mode discharges and the improvement of the target plates. However, the limiting factor still is the overheating of the target plates. This happens either through a slow heating of the tiles or on a fast time scale triggered by MHD activity.

With the expected improvement of the target plate conditions when JET is operated with the new pumped divertor, it is likely that future high performance discharges will reach values of β close to or larger than the Troyon limit. In that case the maximum beta will be limited by MHD instabilities instead of the overheating of the target plates.

In this section we investigate the global MHD stability limits of the new JET divertor geometry. In this new geometry the shape of the plasma boundary changes considerably. Firstly, the minor radius decreases from typically 1.1 m to 0.86 - 0.95 m. Secondly, the plasma becomes more elongated with a single X- point at the bottom. Also the triangularity is considerably reduced. The effect of a smaller minor radius is to increase the maximum beta (at a constant total current and magnetic field). Reducing the triangularity will, especially for the relatively peaked pressure profiles, have a large destabilizing effect [7]. The effect of the X-point is to increase the shear locally near the plasma edge which is stabilizing both for ballooning modes and the external kink. The combined effect of the changes in the plasma geometry on the stability limit is not predictable and requires detailed calculations using the full divertor geometry. In the following, the results are given of the stability calculations of the ideal MHD $n \rightarrow \infty$ ballooning modes and the $n = 1$ external kink mode.

2.1 Method

The usual procedure to calculate the MHD stability boundaries is, given a shape of the plasma boundary, to define a class of pressure and q- profiles with a limited number of parameters and to find the maximum β stable to high-n ballooning modes and the $n = 1$ external kink mode within this class. This leads, in general, to broad pressure profiles with large gradients near the edge combined with q-profiles which are relatively flat in the plasma centre and have large shear near the boundary. This type of profiles has little resemblance with the peaked profiles in the JET high performance discharges.

Here, we will not try to do a full MHD stability study of all plasma parameters and profiles possible. Instead we take one particular JET discharge which is relatively close to the Troyon limit and use this as a reference case. In this way we are assured that the pressure and q-profiles used in the stability analysis are relevant for the JET high performance discharges. The equilibrium is reconstructed from the magnetic measurements and the pressure profile using the IDENTD equilibrium identification code [8].

Starting from this equilibrium, the pressure gradient is increased in small steps until the pressure profile is marginally stable to ballooning modes over the whole plasma. During the iteration the q-profile is kept as constant as possible under the constraint of a constant total current. This procedure yields the maximum β stable to ballooning modes under the constraint of the experimental q-profile, the total current and the toroidal magnetic field. For the ballooning stability calculations the HBT stability code [9, 10] is used. To determine the stability boundary of the $n = 1$ external kink mode, the total pressure of the reference discharge is increased in steps but now both the q-profile and the shape of the pressure profile are kept fixed. To avoid the $m/n = 1/1$ internal kink becoming unstable, the q-profile is slightly broadened such that q on axis is 1.05. The CASTOR code [5] is used for the $n = 1$ stability calculations. The equilibrium quantities needed as input for the CASTOR code are calculated with the HELENA code [6].

Once the stability boundaries of the reference case with the old X-point geometry are established, the shape of the plasma is changed to the new divertor plasma shape. Starting from the same set of pressure and q- profiles, again the stability boundaries of the ballooning modes and the $n = 1$ external kink mode are calculated.

To enable the stability calculations of the up-down asymmetric plasma shape of the divertor geometry both the CASTOR and HELENA codes have been extended. The new versions of the two codes are described in appendix A and B.

2.2 Ideal MHD stability limits

As the reference discharge, we use the JET discharge with the highest performance, discharge #26087 in which an equivalent Q_{DT} of 1.14 was obtained [3]. The time slice is taken at t=53.3s just before the phase of good performance ends with a 'carbon bloom'. At this time, β is at 80% of the Troyon limit. The plasma is operated as a single X-point plasma, although the up-down asymmetry of the plasma boundary is small (see Fig. 2.1). Some relevant plasma parameters are listed in table 2.1. The pressure and the q-profile are shown in Fig. 2.2.

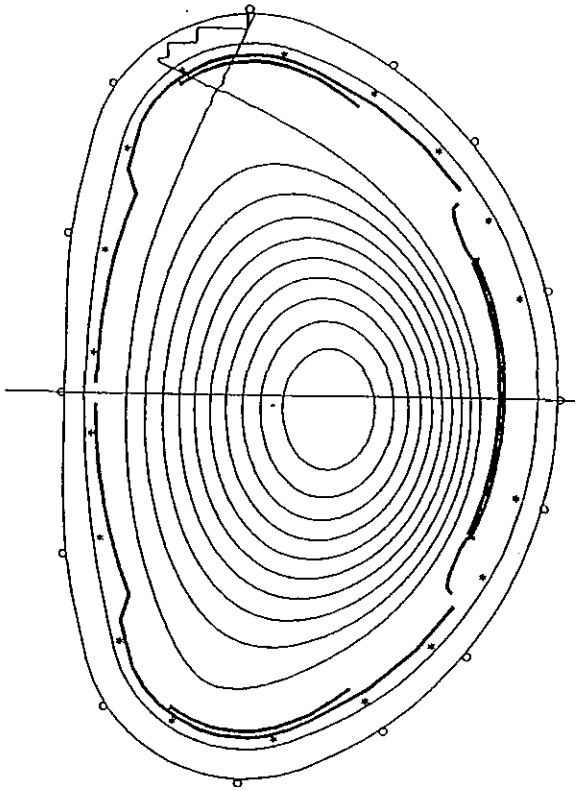

Fig. 2.1 *The plasma shape of the JET discharge 26087.*

The result of the optimization of the pressure profile with respect to ideal $n \rightarrow \infty$ ballooning modes is shown in Fig. 2.3. The figure shows a comparison of the measured profile gradient and the marginally stable profile. Also included is the pressure profile as obtained from the equilibrium reconstruction which was used as the starting point. It is clear that the pressure gradients in this discharge are, even locally, almost a factor of two away from the maximum pressure gradient. Only in the centre of the plasma, is the plasma close to the stability boundary. However, this occurs in the region where $q < 1$ where unstable ballooning modes would have very large toroidal mode numbers, $n > 100$.

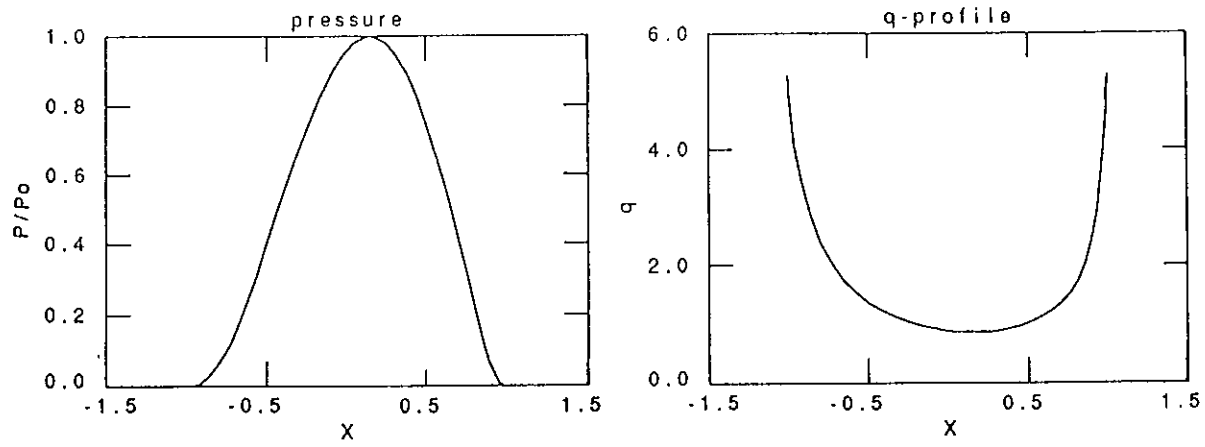

Fig. 2.2 *The pressure profile and the q- profile of discharge 26087, at t=53.3s.*

These high n values are probably not relevant. The pressure profile is not optimized beyond $\psi > 0.90$ because this would lead to unphysically large current density gradients near the plasma edge. The value of β for the marginally stable equilibrium is 4.3% which has to be compared with the 2.4% of the actual discharge. The corresponding Troyon factor $g = \beta/\beta_N = 4.1$ with $\beta_N = I/aB$.

The maximum β stable to the $n = 1$ external kink mode is much larger than the ballooning limit for this discharge, $\beta = 7.2\%$. This is due to the shape of the current density profile which has only a small gradient near the plasma boundary. The resulting $n = 1$ kink instability has a global character with a large amplitude across the plasma, see Fig. 2.4. This is typical for the $n = 1$ kink at high β and is very different from the so-called peeling modes which are more driven by the local current density gradient at the edge. Thus, although the high performance discharge #26087 reaches 80% of the Troyon limit, the stability calculations for this specific discharge show that the actual limit is closer to 4.3% and is determined by ballooning mode stability.

With the new pumped divertor in the JET vacuum vessel, a number of possible plasma shapes have been defined. In this section we will discuss the stability properties of two different shapes : the so called 'slim' and the 'fat' case. The two plasma shapes are plotted in Fig. 2.5. The slim plasma shape is characterized by a larger connection length and will be used primarily for divertor studies. The fat plasma shape has a larger volume and will be used in the performance optimization studies.

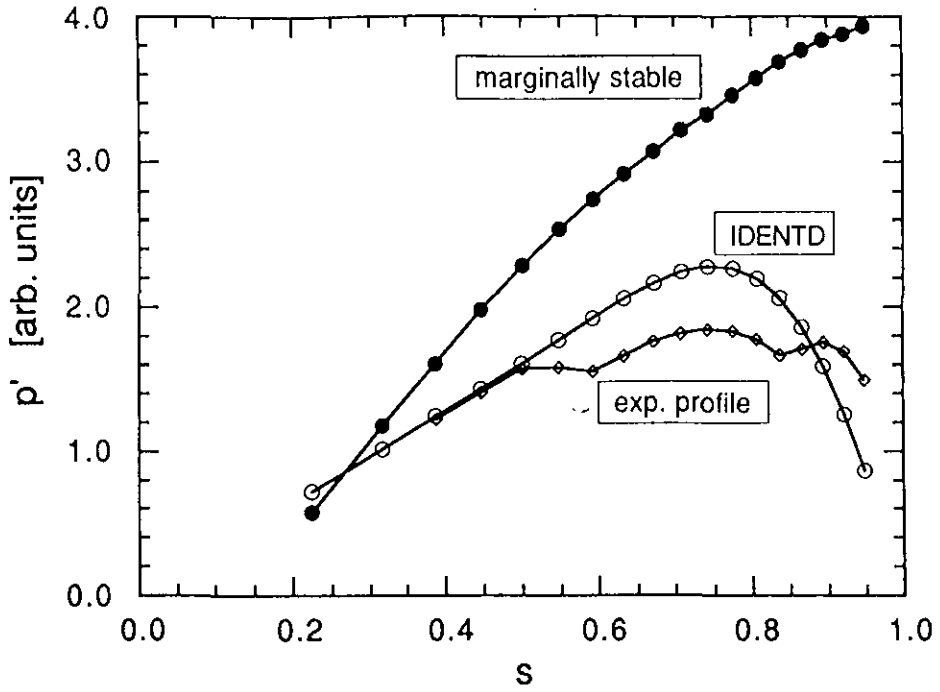

Fig. 2.3 *The profile of the marginally stable pressure gradient as a function of* $s = \sqrt{\psi}$. *Included are the experimental profiles of the pressure gradient from LIDAR and as reconstructed by IDENTD.*

The equilibrium of the new divertor geometries is constructed by using the profile shapes the same as in the reference case but now with a total current of 3 MA and a vacuum magnetic field of 3 T. The results of the ballooning mode optimization for the slim and the fat plasma shapes give a similar profile as is shown in Fig. 2.3 for discharge 26087, the reference case. The maximum β stable to ballooning modes is $\beta_{max} = 4.9\%$ and 4.3% respectively. The difference between the slim and the fat shape appears much less when the maximum β is expressed in the Troyon factor g. In the slim case with the smaller minor radius g equals 4.2 and in the fat case 4.1.

shape	magnetic field [T]	current [MA]	inverse aspect ratio	β_{max} ballooning	β_{max} external kink
26087	2.87	3.17	0.357	4.3	7.2
slim	3.0	3.0	0.302	4.9	3.8
fat	3.0	3.0	0.332	4.3	4.8

Tabel 2.1 *The stability limits for ballooning modes and the* $n = 1$ *external kink mode for three JET plasma shapes.*

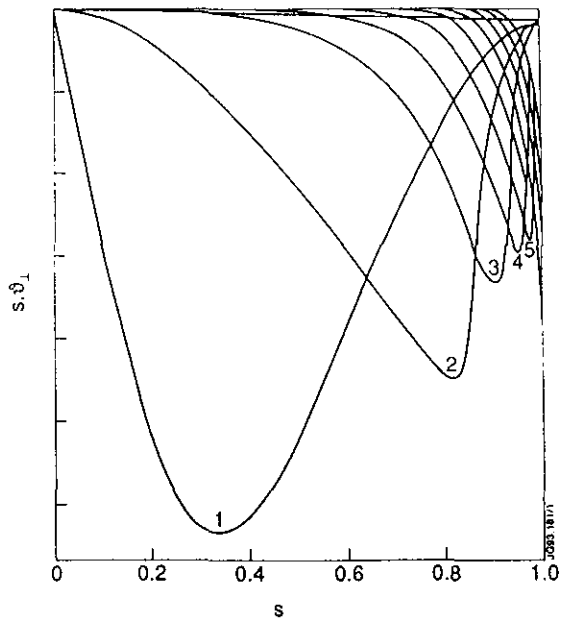

Fig. 2.4 *The mode structure of the $n = 1$ external kink mode at high β.*

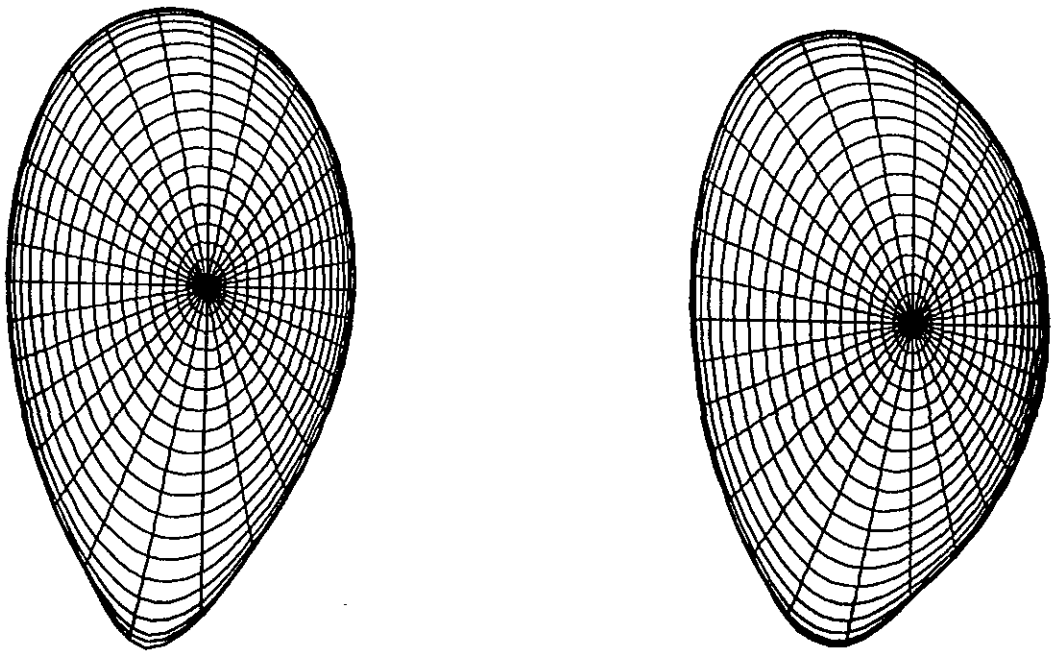

Fig. 2.5 *The new JET divertor plasma shapes, the 'slim' and the 'fat' configuration.*

The changes in the plasma shape have a much larger influence on the stability of the $n = 1$ external kink mode. The maximum values of β stable to the external kink mode are 3.8% and 4.8% for the slim and the fat case respectively. In both cases the mode structure of the kink mode has the same global structure as that shown in Fig. 2.4. This type of external kink cannot easily be stabilized by a small local change in the current density profile at the edge and the stability limit found will therefore not be very sensitive to local changes at the edge.

So, in the case of the slim plasma shape with a large ellipticity and almost no triangularity, the stability limit of the external kink mode is significantly lower than the ballooning limit. This will lead to a different manifestation of the β limit in the experiment. In the present high β experiments at JET large sawteeth and ELMs cause the degradation of confinement [11]. Also, the pressure profile is sometimes, locally, close to the ballooning boundary. Ballooning modes can however not be directly observed and their effect is to keep the pressure gradient below the marginal value. In the case of the slim plasma shape the first mode to become unstable with increasing β is a global external kink mode, which will lead to a disruption.

3. MHD STABILITY OF FREE BOUNDARY RESISTIVE LOW-N MODES

3.1 Introduction

The MHD instability underlying the edge localized modes as occur during the H-mode phase of a plasma, has not yet been satisfactorily identified. This is made more difficult by the local nature of the mode, the instability is driven by the local steepening of the density and temperature profile at the plasma boundary during the H-mode. For the MHD stability calculations, measurements of the local details of the equilibrium profiles of the pressure and the current density are essential, but especially for the current density profile difficult to obtain. Also, due to the high frequency of the ELM precursor, typically > 50 kHz, not many diagnostics are able to observe the instability.

In [12] the 'giant' ELMs (type I), as observed in DIII-D close to the β limit, were attributed to ideal MHD ballooning modes. More recently however it was suggested that although the local pressure gradient is marginally stable to ideal ballooning modes, this only limits the maximum pressure gradient. It is probably not the actual cause for the giant ELMs. The smaller so-called type III ELMs generally occur well below the ideal ballooning limit. Also in JET, the pressure gradient at the plasma boundary is in most cases well below the ideal ballooning limit.

An important clue for the identification of the ELM is its dependence on the parameters influencing the resistivity at the plasma boundary. ELMs can be triggered by lowering the edge temperature by gas puffing and they can be stabilised by heating the plasma edge. ELMs are also triggered by a strong impurity influx into the plasma. From this dependence of the occurrence of ELMs on the parameters influencing the edge resistivity it is concluded that the ELM is a resistive MHD mode.

In JET discharges, *Resistive* ballooning modes have been shown to be close to their stability limit for relatively low values of the toroidal mode number ($n \sim 10$) [13]. However, the ELM causes a large perturbation of the plasma boundary and an expulsion of particles and energy from the plasma edge. This behaviour is not expected from the radially localized ballooning modes. In [2,4] it is proposed that low-n free boundary resistive modes are the relevant instabilities underlying the ELM. The $n = 1$ free boundary resistive modes, i.e. the resistive equivalent of the ideal external kink mode, are mostly driven by edge current density and its gradient. The edge current density can be large in H-mode discharges due the bootstrap current driven by the large edge pressure gradient. These modes have a larger radial extension over more than one rational surface and cause a large

perturbation of the plasma boundary. In a study of the stability of the $n = 1$ free boundary tearing mode of a JET elmy H- mode equilibrium it was shown that a small change in the current profile at the edge, increasing the edge current density gradient, can drive this mode unstable. Also, a critical value of the resistivity exists below which the mode is stabilised due to the favourable average curvature.

In [14] the stability of the $n = 1$ ideal external kink mode is investigated in a circular geometry. There, it is proposed that the ELM is an ideal kink mode driven unstable by the enhanced current density. In JET discharges, however, it is found that the $n = 1$ ideal external kink mode is very stable due to the high shear at the plasma edge. The resistive kink modes are much easier driven unstable.

In this chapter we will extend our previous study [4] in two directions. Firstly, higher values of the toroidal mode number ($n = 1..4$) are studied. This is motivated by the observations in ASDEX of poloidal mode numbers of the order of $10 - 15$ in a discharge with q at the boundary of 3.3. This would mean that the toroidal mode numbers must be of about $n = 3 - 5$. Secondly, the influence of the edge pressure gradient which will be more important for the higher mode numbers is investigated.

3.2 Resistive low-n mode stability of JET H-mode equilibria

The influence of the local pressure profile on the stability of resistive modes localized at the plasma edge can be twofold. The pressure gradient is a driving force for instabilities like low-n resistive ballooning modes. However, a large edge pressure gradient also implies a large pressure at the particular mode rational surface. The pressure itself in combination with the favourable average curvature has a stabilizing effect on the free boundary tearing (resistive kink) modes. This effect is particularly pronounced at low values of the resistivity.

In the previous study of the $n = 1$ free boundary resistive kink mode, it was found that at a relatively high value of the resistivity of $\eta = 10^{-5}$, increasing the pressure gradient while keeping the driving current density gradient constant had a stabilizing effect. Increasing the pressure gradient by a factor two, yielded a growth rate of about a factor of two lower. A further increase of the pressure gradient had no effect on the growth rate. No destabilizing effect was found for the $n = 1$ mode.

In this section we will investigate the influence of the edge pressure gradient for the $n = 1$ to 4 resistive free boundary modes. As a starting point we take the JET equilibrium of the H-mode discharge 27793 at $t = 54.08$. In this discharge, ELMs were triggered by a large influx of Beryllium impurities. The equilibrium is calculated with the

IDENTD equilibrium reconstruction code [Blum90]. The resulting profiles of the pressure and the q-profile are plotted in Fig. 3.1. The equilibrium obtained does not have locally large gradients of the pressure and the current density at the edge. This is due to the global nature of the expansion functions used in the reconstruction. Consequently, this equilibrium is stable to all low-n ideal and resistive modes, including the $m/n = 2/1$ tearing mode.

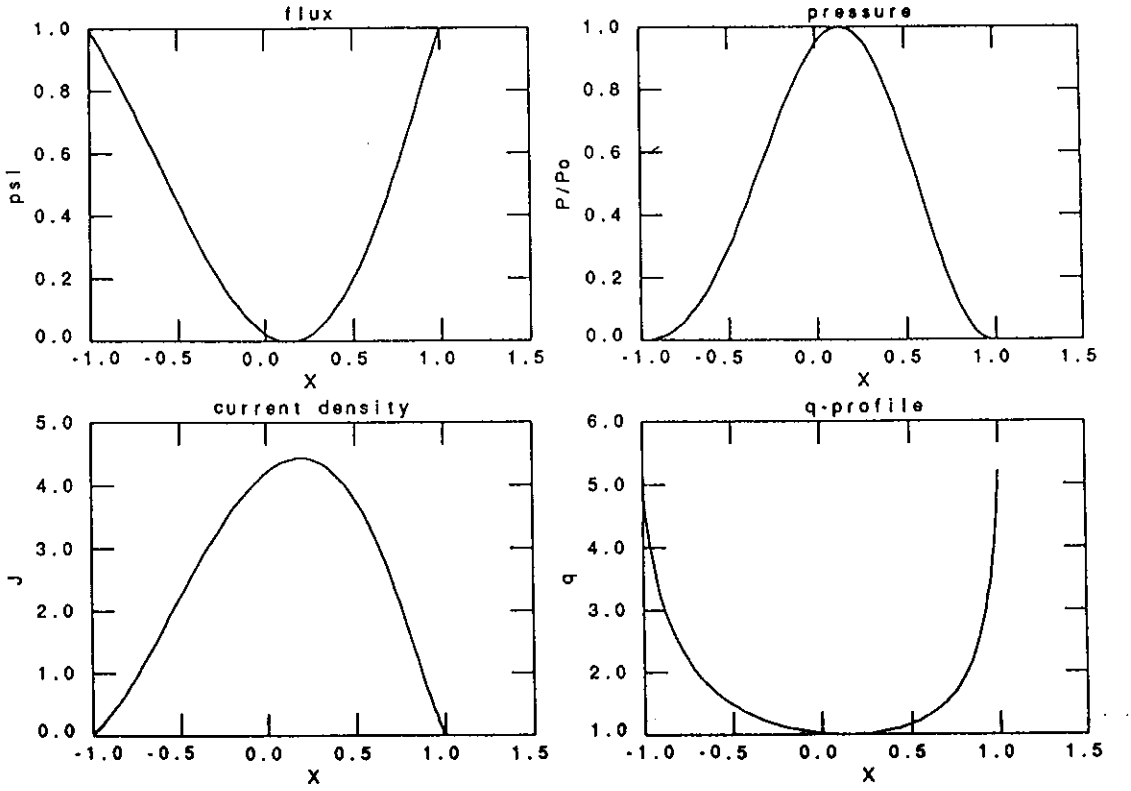

Fig. 3.1 *The equilibrium profiles of discharge 27793 as reconstructed by IDENTD*

To study the influence of the local pressure gradient at the plasma edge, we model the local edge gradients by artificially increasing the pressure gradient up to the point were the plasma becomes unstable. The current driven modes are stable in these equilibria, but above a threshold in the edge pressure gradient, a pressure driven $n = 1$ mode does become unstable. Naturally, this mode shows the opposite behaviour compared to the current driven modes and becomes more unstable with increasing pressure gradient. Also the behaviour with increasing toroidal mode number is different. For the current driven mode the $n = 1$ mode is the most unstable mode. The $n = 2$ mode is already very difficult to excite. The pressure driven mode on the other hand become more unstable with increasing toroidal mode number. This is shown in Fig. 3.2 where the growth rate is plotted as a function of the mode number for three different values of the edge pressure gradient. The

largest pressure gradient in this figure is about one third of the gradient which would be marginally stable to ideal ballooning modes. The resistivity in these calculations was taken at the relatively high value of $\eta = 10^{-5}$. The growth rate is increasing linearly with n and the slope is independent of the pressure gradient for the two cases considered. At the relatively high values of the resistivity, the modes are already unstable for pressure gradients which are much lower than the ideal ballooning limit.

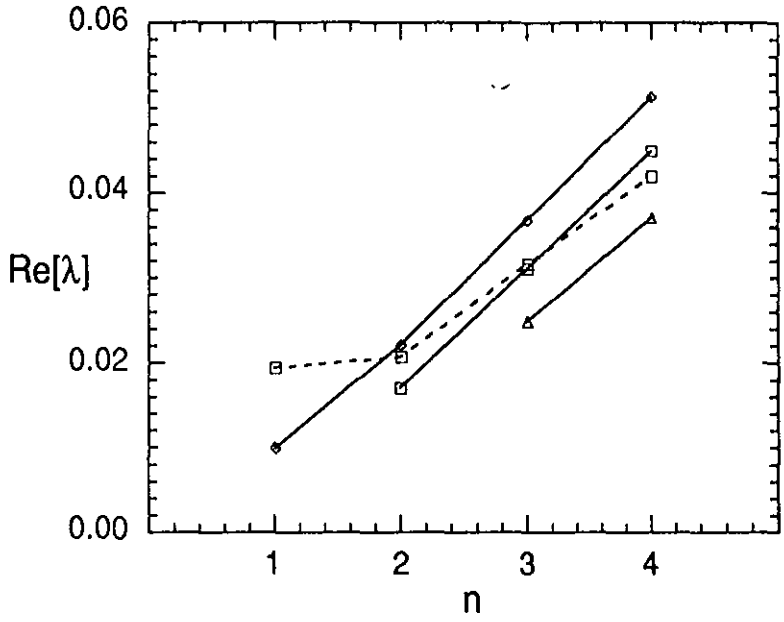

Fig. 3.2 *The growth rates of the $n = 1 - 4$ modes for three different values of the edge pressure gradient. The dashed line corresponds to the case with increased edge current gradient.*

In Fig. 3.3a, the velocity perturbation of the $n = 4$ mode is plotted. The main poloidal mode number is $m = 12$, i.e. the mode is centred around the $q = 3$ surface. Although the calculations are done using a 'free boundary' boundary conditions, the $n = 4$ mode is essentially an internal mode with the largest amplitude at the $q = 3$ surface and almost no perturbations at the plasma boundary. The $n = 4$ mode does not show any significant ballooning effect, the amplitude on in- and outboard side is of comparable magnitude.

With increasing mode number, the density perturbation of the instability, which is equivalent to the plasma compression, decreases. Also the ratio of the parallel to the perpendicular component of the velocity perturbation decreases from about 10 at $n = 1$ to 1 at $n = 4$.

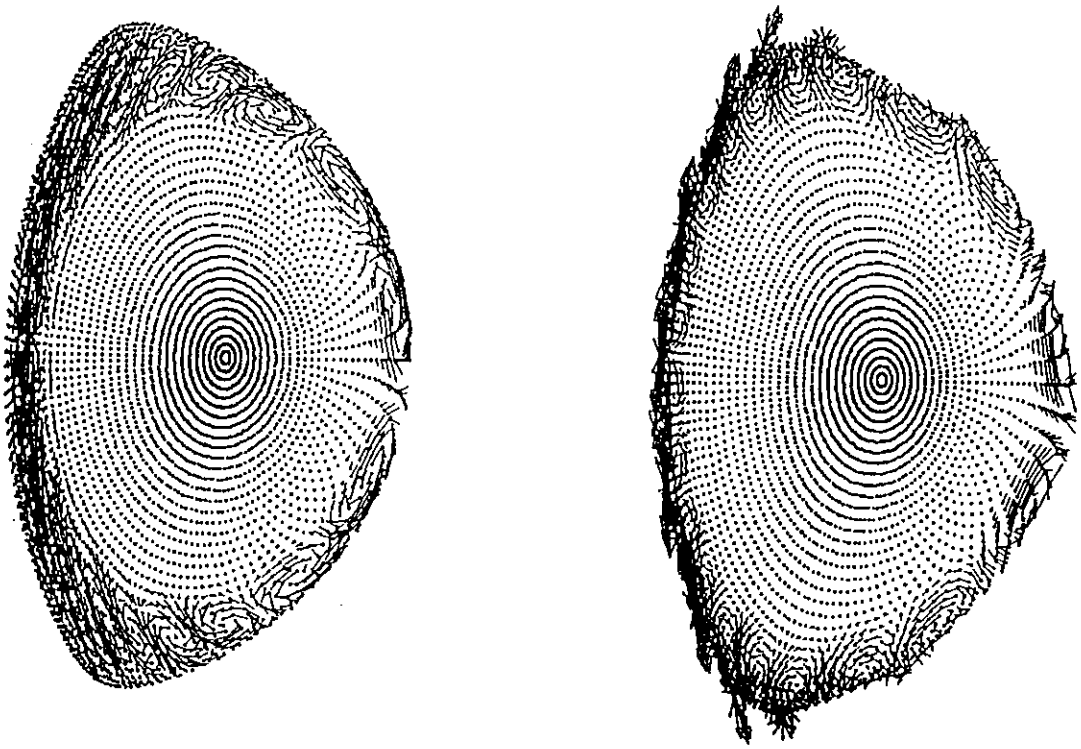

Fig. 3.3 *The poloidal velocity perturbation of the $n = 4$ mode corresponding to* **(a)** *the case with increased pressure gradient ($Re(\lambda) = 4.6 \times 10^{-2}$ in Fig. 3.2) and* **(b)** *of the case with increased edge pressure and current gradient.*

Included in Fig. 3.2 are the growth rates of the low-n modes for an equilibrium with both an increased pressure and a increased current density gradient at the edge. The current density is increased up to the point where the $n = 1$ current driven mode has become unstable. It is clear that the increased current density gradient has the largest effect on the $n = 1$ mode. The $n = 2$ mode is only a little more unstable, the growth rate of the $n = 4$ mode is even lower with the larger current gradient. Although the growth rate of the $n = 4$ mode is only slightly different with the increased current density gradient, the mode structure does change. Due to the increased edge current, the shear at the edge is much smaller. Also the $q = 3$ surface is closer to the plasma boundary. Due to the smaller shear the width of the mode has become larger. The maximum is still at the $q = 3$ surface but in this case the mode does have a large amplitude at the plasma boundary and the free boundary is essential in this case for the instability to occur (see Fig. 3.3b).

With decreasing resistivity, the resistive modes are expected to be stabilized at one point by the favourable average curvature effect which is more pronounced at low resistivity [15,16]. From large aspect ratio theory,.one expects the stabilization to be a weak function of the toroidal mode number. The stabilization increases like $n^{1/3}$. The behaviour of

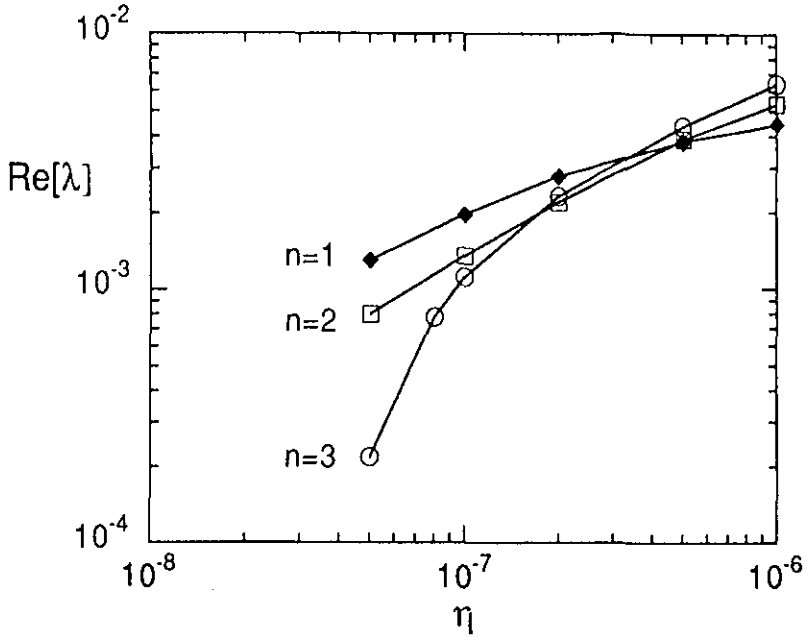

Fig. 3.4 *The growth rates of the $n = 1 - 3$ modes as a function of the resistivity of the case with increased pressure and current gradient at the edge.*

the growth rate of the low-n modes with decreasing resistivity is shown in Fig. 3.4. The growth rate of the higher n modes does decrease faster with increasing n. So, the question of which mode number is the most unstable mode depends sensitively on the actual value of the resistivity. But from the plot it is clear that in the case an ELM is triggered by an rapid increase of the resistivity by some impurity influx, the lowest n will be the first to become unstable.

3.3 Conclusion

At high values of the local resistivity $\eta > 10^{-6}$, low-n modes ($n > 3$) can become unstable at relatively low values of the pressure gradient, even lower as one third of the ideal ballooning limit. However, for the temperatures at the plasma edge in JET H-mode discharges of typically 1 keV, the resistivity is much smaller, $< 10^{-7}$. At these lower values the higher n modes will be more stable due to the stabilizing effect of the average curvature. The most unstable mode number will then depend on the details of the edge pressure and current density profiles. At large edge current gradients the $n = 1$ will be the most unstable. At high pressure gradient, some medium n mode will the most unstable depending on the actual value of the resistivity.

REFERENCES

[1] D. Stork et al, Proc. Int. Conf. on Plasma Physics, Innsbruck 1992, Vol. I, p. 339.

[2] G.T.A. Huysmans, H.J. de Blank, W. Kerner, J.P. Goedbloed, and M.F.F. Nave, Proc. Int. Conf. on Plasma Physics, Innsbruck 1992, Vol. I, p. 247.

[3] The JET TEAM, Nuclear Fusion 32 (2), (1992), p.187.

[4] G.T.A Huysmans, Ph.D. Thesis Free University Amsterdam, 1991

[5] W. Kerner, S. Poedts, J.P. Goedbloed, G.T.A. Huysmans, B. Keegan, and E. Schwartz, Contr. Fusion and Plasma Physics, (1991), 18^{th} Eur. Conf. Berlin, part IV. p.89.

[6] G.T.A. Huysmans, J.P. Goedbloed, and W. Kerner, Proc. CP90 Conf. on Comp. Phys.Proc., World Scientific Publ. Co., (1991), p. 371.

[7] C.G. Schultz, A. Bondeson, F. Troyon, A.Roy, Nuclear Fusion 30, 11 (1990), p. 2259.

[8] J. Blum, E. Lazzaro, J. O'Rourke, B. Keegan, Y. Stephan, Nucl. Fusion 30 (1990), p. 1475.

[9] J.P. Goedbloed, Comp. Phys. Commun. **24**, (1981), p. 311.

[10] G.T.A. Huysmans, R.M.O. Galvao, J.P. Goedbloed, Rijnhuizen Report 90-194, (1990).

[11] Smeulders P. et al., Contr. Fusion and Plasma Heating, (1990), 17th Eur. Conf. Amsterdam, part I, p.323.

[12] Gohil P., Ali Mahdavi M., Lao L., Burrel K.H., Chu M.S., DeBoo J.C., Hsieh C.L., Ohyabu N., Snider R.T. Stambaugh R.D., and Stockdale R.E., Phys. Rev. Lett. **61**, (1988) p.1603.

[13] H.J. de Blank, M.F.F. Nave, W. Kerner, and G.T.A. Huysmans, Theory of Fusion Plasmas, (editors E. Sindoni and J. Vaclavik), (1992), p.343.

[14] J. Manickam, Phys. Fluids B 4, (1992), p. 1901.

[15] Glasser A.H., Greene J.M., and Johnson J.L., Phys. Fluids, **18**, (1975), p. 875.

[16] Hastie R.J., Sykes A., Turner M., and Wesson J.A., Nucl. Fusion, **17**, p.515, (1977).

[17] Soloviev L.S., in : Reviews of plasma Physics, vol. 6, ed. M.A. Leontovich (Consultants Bureau, New York), 1975, p.257.

[18] G.T.A. Huysmans, J.P. Goedbloed and W. Kerner, Phys. Fluids. B, **5**, (1993), p.1545.

APPENDIX A. HELENA

The axisymmetric equilibrium code HELENA [6] was developed for the specific purpose of calculating the equilibrium quantities and the metric coefficients of the flux surface coordinate system as is used in the spectral resistive MHD code CASTOR [5]. In the calculation of the spectrum of a given equilibrium, the actual eigenvalues are the result of a cancellation of stabilizing and destabilizing terms which can be large compared to the actual eigenvalues. Therefore, the equilibrium data have to be known very accurately.

In HELENA, a high level of accuracy is obtained by means of bicubic Hermite finite elements. This leads to a continuous representation of both the flux and magnetic field across the poloidal plane. The shape of the plasma boundary is approximated using an isoparametric mapping of the curved finite elements aligned with the boundary onto a rectangular grid of finite elements. In the isoparametric mapping the same bicubic Hermite elements are used. This results in a numerical error in the flux which scales with the fourth power of the size of the finite elements. The error in the magnetic field scales with the third power. The isoparametric mapping can also be used to adjust the grid of finite elements such that the element boundaries are aligned onto the centred flux surfaces. In this way a inverse representation of the equilibrium is obtained i.e., x and y as a function of the flux ψ and of the angle, instead of the usual representation $\psi(x, y)$. This greatly facilitates the calculation of the metric coefficients of the straight field line coordinate system as used in the CASTOR code.

The new version of HELENA includes the possibility of non up-down symmetric shapes of the plasma boundary, so that single x-point plasma shapes can now also be represented. In the case of an up-down symmetric plasma, the Grad- Shafranov equation had to be solved only in the upper or lower half of the poloidal plane with an additional natural boundary condition along the axis of symmetry. Obviously, in the general asymmetric case, the equilibrium equation has to be solved in the whole poloidal plane (inside the plasma boundary) without the additional boundary condition. Also, the position of the magnetic axis, which was located on the axis of symmetry in the symmetric case, can now be in any one of the finite elements. To find the magnetic axis requires the solution of a set of two second order polynomials in each finite element to find the minimum value of the flux in each element.

To test the accuracy of the new up-down asymmetric version of the HELENA code, the results of HELENA are compared with an analytic expression for an up- down asymmetric equilibrium. To that end we have extended [10] the well- known Soloviev [17]

equilibrium to include asymmetric shapes of the plasma boundary. The general expression of the up-down asymmetric Soloviev equilibria is given by

$$\begin{aligned}\psi(x,y) = (x - \tfrac{1}{2}\epsilon(1-x^2))^2 + \frac{1-\frac{1}{4}\epsilon^2}{1-\tau}((1+\epsilon x)^2 - \tau)(\frac{y^2}{bc}) \\ + \frac{2}{\epsilon}(1-\frac{1}{4}\epsilon^2)\frac{b-c}{bc}(x - \frac{1}{2}\epsilon(1-x^2))y \ ,\end{aligned} \tag{A.1}$$

where ϵ is the inverse aspect ratio, $\sqrt{bc}$ is the ellipticity, $(b-c)/\sqrt{bc}$ is a measure of the up-down asymmetry, and τ measures the triangularity. The shape of the plasma boundary is given implicitly by $\psi(x,y) = 1$.

An example of an asymmetric Soloviev equilibrium is shown in Fig. A.1. The parameters of this equilibrium are given by $\sqrt{bc} = 1.5, (b-c)/\sqrt{bc} = 0.03, \epsilon = 0.25$, and $\tau = 0$.

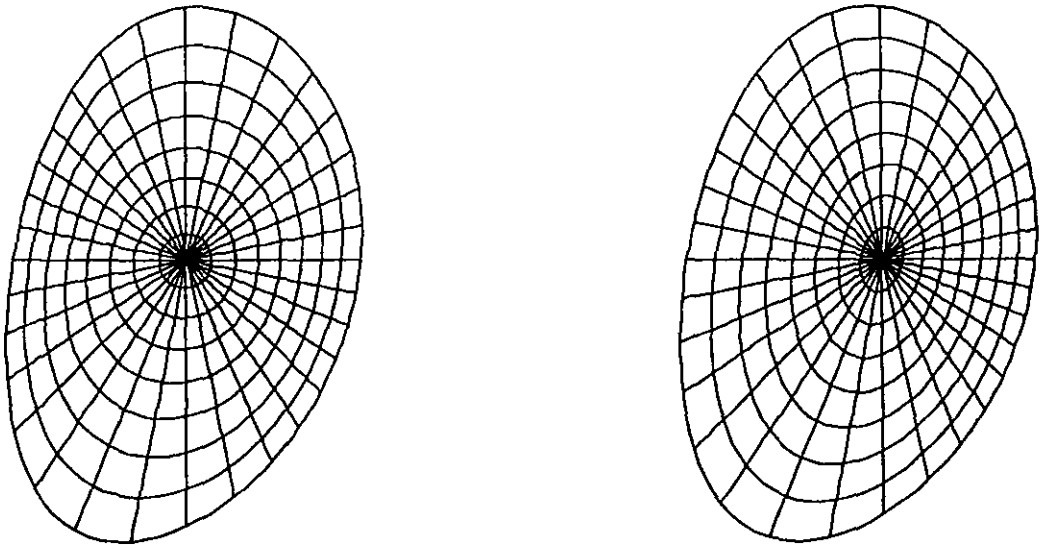

Fig. A.1 (a) *The initial grid of bicubic Hermite finite elements of an asymmetric Soloviev equilibrium.* **(b)** *The final grid of elements aligned on flux surfaces.*

The initial grid of curved finite elements is plotted in Fig.A.1a. Notice that the shapes of the coordinate surfaces change from the shape of the plasma boundary to a

circular shape in the plasma centre. Fig.A.1b shows the final grid in which the finite elements are aligned on flux surfaces. The relative error in both the flux and the gradient of the flux as a function of the number of radial finite elements is plotted in Fig. A.2. As expected, the error in the flux scales with the fourth power of the grid size, the gradient of the flux scales with the third power.

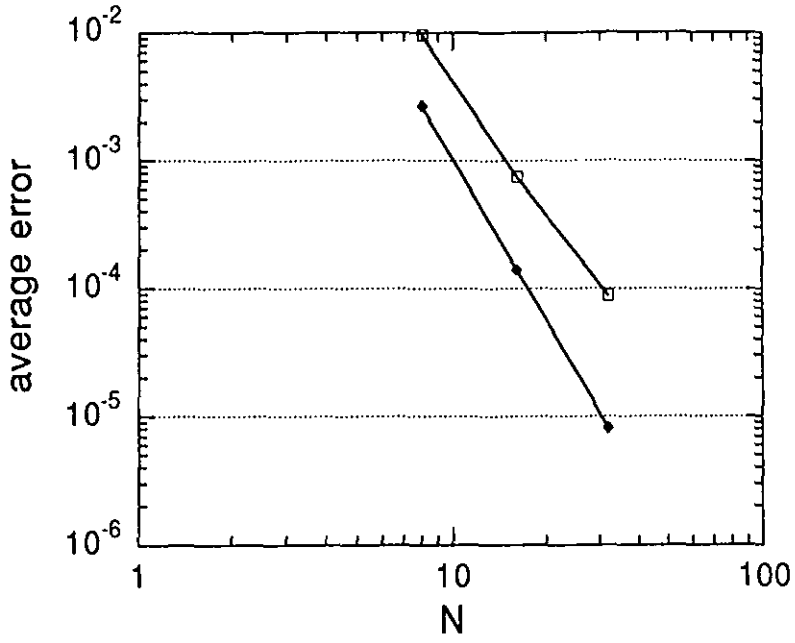

Fig. A.2 *The convergence of the average error over 100 points in each finite element as a function of the number of finite elements.*

APPENDIX B. CASTOR

For the study of the ideal and resistive stability of JET discharges the CASTOR [5] code is used. In the CASTOR code the linearized resistive compressible MHD equations are solved in a general toroidal geometry.

The eight variables, the temperature, the density, and the velocity and the vector potential vectors, are discretized using cubic and quadratic finite elements in the radial direction and Fourier harmonics in the poloidal angle. The Galerkin method used results in a non-Hermitian eigenvalue problem with large sparse matrices. Inverse vector iteration is used for the calculation of single eigenvalues, whereas the QR algorithm can be used to compute the complete spectrum. Due to the localized nature of the finite elements, the CASTOR code can easily resolve the narrow layers of the resistive modes at the low values of the resistivity relevant in present day tokamaks ($\eta \sim 10^{-9} - 10^{-10}$).

More recently, the CASTOR code was extended to include a vacuum surrounding the plasma so that also the stability of free boundary modes can be investigated [18]. To enable the study MHD stability of the new JET divertor plasma shapes (see chapter 2), the CASTOR code is extended. The new version of CASTOR now uses the up-down asymmetric equilibrium data from the new version of the HELENA equilibrium code as described in the previous section.

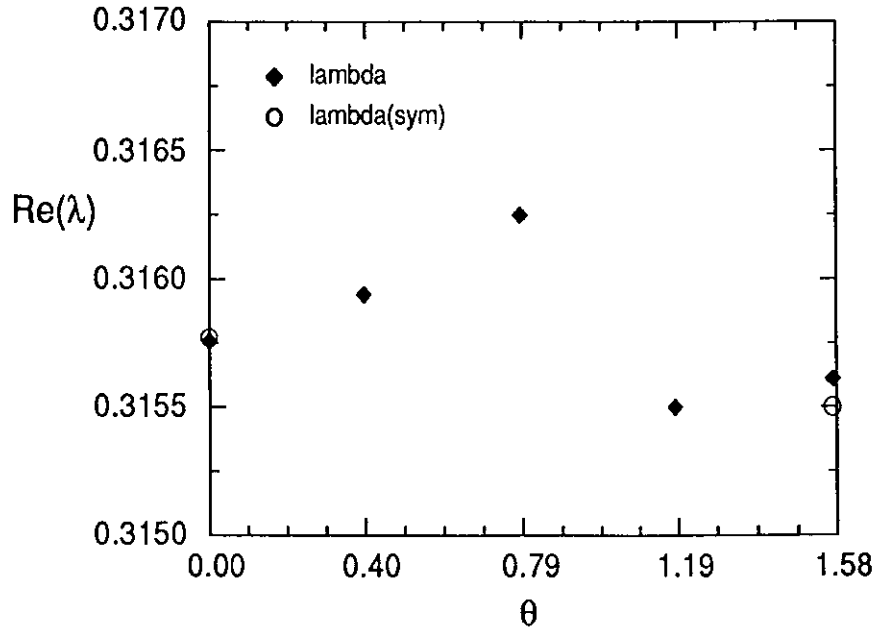

Fig. B.1 *A test case for the up-down asymmetric version of CASTOR: the growth rates of a rotated ellipse at small inverse aspect ratio,* $\epsilon = 0.01$.

As a test case for the up-down symmetric versions of HELENA and CASTOR, the growth rate of the $n = 1$ ideal external kink mode in an (almost) straight elliptical plasma is calculated. The eigenvalue should then be independent of the orientation of the ellipse. The resulting growth rates are shown in Fig. B.1 for a number orientations of the ellipse. The angle θ in this figure is the angle between the longer axis of the ellipse with the vertical. The ellipticity is 1.5 and the inverse aspect ratio is 0.01. Included are the eigenvalues of the up-down symmetric CASTOR version for the two symmetric orientations. The relative variation in the eigenvalue is about $2{\times}10^{-3}$ which has to be compared with the variation due to the finite inverse aspect ratio of 0.01. The effect of the up-down asymmetry due to the ellipticity of 1.5 is much larger than the finite aspect ratio of 0.01. This shows that both the new versions of the HELENA equilibrium code and the stability code CASTOR give correct and accurate results for general up-down asymmetric shapes of the plasma boundary.

The interface program between the IDENTD equilibrium reconstruction and the HELENA code has also been extended to handle arbitrary plasma shapes. This enables the MHD stability analysis of the new up-down asymmetric JET divertor plasmas.